JCTC Journal of Chemical Theory and Computation

Real-Time TD-DFT Simulations in Dye Sensitized Solar Cells: The Electronic Absorption Spectrum of Alizarin Supported on TiO_2 Nanoclusters

Rocío Sánchez-de-Armas, Jaime Oviedo López, Miguel A. San-Miguel, and Javier Fdez. Sanz*

Department Physical Chemistry, University of Seville (Spain)

Pablo Ordejón and Miguel Pruneda

CIN2—Centre d'Investigació en Nanociència i Nanotecnologia (CSIC-ICN), Campus UAB, 08193 Bellaterra, Spain

Received June 2, 2010

Abstract: The structural and electronic properties of the alizarin dye supported on TiO_2 nanoclusters have been examined by means of time-dependent density-functional (TD-DFT) calculations performed in the time-domain framework. The calculated electronic absorption spectrum of free alizarin shows a first band centered at 2.67 eV that upon adsorption features a red shift by 0.31 eV, in agreement with both experimental and previous theoretical work. This red shift arises from a relative stabilization of the dye LUMO when adsorbed. To analyze the dependence of the electronic properties of the dye-support couple on the size of metal-oxide nanoparticles, different models of $(TiO_2)_n$ nanoclusters have been used (with $n = 1$, 2, 3, 6, 9, 15, and 38). As a conclusion, the minimal model is good enough to theoretically reproduce the main feature in the spectrum (i.e., the energy shift of the main band upon binding to TiO_2). However, it fails in creating intermediate states which could play a significant role under real experimental conditions (dynamics of the electronic transfer). Indeed, as the size of the nanocluster grows, the dye LUMO moves from the edge to well inside the conduction band (Ti 3d band). On the other hand, to assess the consistency of the time-domain approach in the case of such systems, conventional (frequency-domain) TD-DFT calculations have been carried out. It is found that, as far as the functional and basis set are equivalent, both approaches lead to similar results. While for small systems the standard TD-DFT is better suited, for medium to large sized systems, the real-time TD-DFT becomes competitive and more efficient.

1. Introduction

Dye sensitized solar cells (DSSC) have attracted considerable attention in recent years.[1] They are based on transition metal derivatives or organic dye molecules that are adsorbed on a semiconductor, generally a metal oxide such as TiO_2. The photochemical properties of different sensitizers have been extensively investigated, in an attempt to design dyes with maximal visible light absorption coupled to long-lived excited states. Ruthenium dyes are the most efficient sensitizers in DSSCs by now, although they have some disadvantages. Molecular modification of these dyes is an arduous task due to their complicated synthesis routes, and the materials involved in the synthesis procedures are rather expensive. In contrast, organic dyes have a much lower cost, and their molecular design is more convenient and easier. They have large absorption coefficients due to intramolecular $\pi \rightarrow \pi^*$ transitions, and there are no concerns about limited resources, because they do not contain noble metals such as Ru.

* Corresponding author e-mail: sanz@us.es.

10.1021/ct100289t
Published on Web 08/16/2010

A key process in the operation of this kind of devices is the charge injection from the dye molecule adsorbed at the nanoparticle surface to the conduction band states of the semiconductor. The injection rate has been found to depend on the electronic properties of both the dye and the semiconductor, as well as the distance between them.[2] The DSSCs can be classified into two types, depending on the electron injection mechanism from the dye to the semiconductor. In type-I cells, the injection mechanism is indirect and first involves the photoexcitation to an excited state of the dye, from which an electron is transferred to the conduction band of the semiconductor. In contrast, type-II cells involve a direct mechanism or a "one-step" electron injection from the ground state of the dye to the conduction band of the semiconductor. A new charge-transfer band that, upon adsorption, appears in the electronic absorption spectrum of the dye reveals the direct injection mechanism, whereas in the case of an indirect mechanism, no new bands are seen in the spectrum.[1,3]

Alizarin is an organic molecule that has been investigated in great detail as a photosensitizer, with high incident photon-to-current conversion efficiencies.[1−7] The electron injection from the alizarin excited state into TiO_2 proceeds at an ultrafast 6 fs time scale.[8,9] The experimental electronic absorption spectrum for free alizarin shows a low energy band centered at 2.88 eV (431 nm) and other, stronger bands at energies higher than 5 eV (250 nm) with a shoulder at 3.82 eV (325 nm). Upon adsorption, the lowest band is red-shifted by about 0.4 eV and appears at 2.47 eV (503 nm), which is characteristic of an indirect mechanism. The other bands are also shifted and appear at energies higher than 3.55 eV (350 nm).[4]

An important issue of this process is the nature of the excited states, in particular, whether the photoexcitation results in a state mainly localized at the chromophore, i.e., a locally excited state, or a state that is mainly localized at the titanium, i.e., a charge-transfer state. Another issue under discussion is whether the electron transfer (ET) mechanism is adiabatic or nonadiabatic.[1,2,6,10] In the adiabatic mechanism, the coupling between the dye and the semiconductor is large, and ET occurs through a transition state along the reaction coordinate that involves a concerted motion of nuclei. During an adiabatic transfer, the electron formally remains in the same Born−Oppenheimer (adiabatic) state that continuously changes its localization from the dye to the semiconductor along the reaction coordinate. Nonadiabatic effects decrease the amount of ET that happens at the transition state but open up a new channel involving direct transitions from the dye into the semiconductor that can occur at any nuclear configuration. In this case, a strong coupling is unnecessary as a large density of TiO_2 acceptor states can still give rise to an ultrafast injection even when the coupling is weak. The nonadiabatic ET effect is a quantum effect and, similar to tunnelling, shows exponential dependence on the donor−acceptor separation.

Theoretical methods are a powerful tool for molecular design, and conclusions drawn from calculations are valuable guidelines for the synthesis of new efficient dyes. Time-dependent density functional theory (TD-DFT) has been usually chosen to reproduce the electronic absorption spectra of organic dyes. This method provides an improved treatment of the electron correlation effects relative to other methods like CIS.[4] Nevertheless, calculations with conventional linear response (LR) TD-DFT implementation in the frequency domain[11] to estimate individual excitations are computationally demanding, and the results are limited to relatively small models. The alizarin molecule is one of the smallest sensitizer dyes, and that makes it a good system to be theoretically investigated.[12,13]

In previous work by Duncan and Prezhdo,[4] the free and adsorbed alizarin spectra were calculated using TD-DFT. A minimal model was used in which the dye molecule was bound to a single Ti atom and a set of water and hydroxyl ligands. An essentially localized excitation of the dye followed by an electron transfer to a localized surface state and a spreading into the conduction band states were suggested. Results from this and similar work[12] are able to qualitatively show the main features of experimental spectra, and the effect of bounding alizarin to the surface, but they are limited in size and make it difficult to fully assess the role of electronic delocalization into the clusters. In addition, extensive theoretical studies on the charge transfer dynamics have been performed.[1,6,13] From these works emerged the conclusion that the adiabatic mechanism was more dominant relative to the nonadiabatic one. Recent experimental work,[7] however, concluded that finite size effects produce a multiple electron injection with different time scales, which is characteristic of a nonadiabatic event.

In this work, we report on density functional theory (DFT) calculations on the alizarin molecule isolated and adsorbed on TiO_2 clusters. First, we consider the geometry of the organic dye in the electronic ground state as well as the geometries of the dye-cluster models. Second, we explore the optical response of the different structures using TD-DFT. These calculations are performed in a complementary way through the conventional linear response approach[14] and through real time propagation[15,16] with a basis of localized orbitals. One important initial goal of this work is to establish the accuracy of the real time TD-DFT method within the SIESTA code in the case of organic dyes. For this reason, we have chosen a molecule that has been extensively studied. Since the cost of this method is relatively low, we are able to extend the study to moderately large systems that are closer to experimental conditions. The aim in this case is to analyze the electronic structure as the cluster size increases and how this affects to the theoretical spectra. We will focus on the delocalization of the excited electrons into the clusters and how it might play a significant role in the process. We conclude that the real-time TD-DFT calculated absorption spectra are in good agreement with the experimental results, in terms of both absolute absorption energies and relative band intensities. Moreover, it is shown that, although a minimal model can account for the qualitative features of the spectra, it might be too limited in describing the electronic structure of the system, which is essential in describing the dynamics of the electron transfer.

2. Computational Methods

2.1. Models. The system to be studied involves an organic molecule that is adsorbed on TiO_2 nanoparticles suspended in an electrolyte. It is often implicitly assumed that each experimental absorption peak corresponds to a single adsorption geometry. However this does not necessarily have to be the case. For instance, there could be differences in the cluster size, adsorption sites, alizarin isomers, etc., so the actual spectra would be the average of an enormous ensemble of states.[3] Here, we present a set of models that try to cover the main aspects of this issue.

The majority of the experimental studies on the interfacial ET in the dye sensitized TiO_2 systems are carried out with TiO_2 nanoparticles that are a mixture of the rutile and anatase crystal forms of TiO_2 with a variety of exposed surfaces. However, many experimental studies use colloidal TiO_2 particles that are prepared by the hydrolysis of $TiCl_4$ in cold water. The anatase phase becomes more stable than the rutile phase when the sizes of TiO_2 clusters are smaller than 14 nm.[17]

It is theoretically unfeasible to determine the actual adsorption geometry for the alizarin adsorbed on TiO_2 clusters in solution, as it would be necessary first to know the cluster morphology. We have made calculations adsorbing the alizarin molecule on clusters of several sizes. It is well beyond the scope of this paper to find the absolute energy minimum for the clusters, even more so when the minima could change upon adsorption and/or including solvation effects. The starting geometries for the TiO_2 clusters in this study were taken from the literature. The small models[18,19] are taken from optimized geometries starting from spherically shaped particles, whereas the largest one (U_{38}) started from the anatase structure.[20] We regard these clusters as a reasonable choice for their actual geometries.

The selected models range from a minimal cluster that was used in previous theoretical work to a relatively large one with 38 TiO_2 units. The minimum model (as in ref 4) corresponds to a neutral TiO_4H_4 cluster, which includes a single metal atom. Formally, it can be written as U_1 ($2H_2O$), where U is a TiO_2 unit. In addition, other clusters labeled as U_2, U_3, U_6, U_9, U_{15}, and U_{38} were also considered. The larger cluster has a diameter of about 1 nm that has to be compared to nanoparticles of about 2−6 nm used in experiments, and therefore this model will provide results more comparable to real experiments. However, the use of small clusters is interesting in the study of the effect of delocalization and also helps to establish which is the minimal size to obtain reliable data.

It has been suggested from the infrared data and theoretical structure calculations that catechol, whose structure is similar to that of alizarin, is covalently linked to the surface Ti atom in a chelating bidendate mode involving the oxygen atoms of its two hydroxyl groups. Following Duncan and Prezhdo,[4] the present study uses the bidendate geometry for the adsorbed alizarin as a first working model (Figure 1).

Another crucial aspect is whether the alizarin (or the whole system) is neutral or charged upon adsorption. We have studied two extreme cases for the adsorption: the system was either neutral (denoted as Aliz-2H-Cluster), and therefore the system keeps the two phenolic hydrogen atoms, or dianionic (Aliz-Cluster-2), where these hydrogen atoms were removed. For the neutral case, the hydrogen atoms are linked to cluster oxygen atoms rather than to the alizarin molecule, as preliminary calculations showed that this might be the most stable case, although we did not try every possible adsorption site rearrangement. As shown in Figure 1, in the models we have used, the hydrogen atoms were as separated as possible on the clusters, following the strategy used in ref 13. Again, we should stress that this is only a sensible model for the adsorption. Generally speaking, the neutral models are not appropriate for small clusters, since adsorbing hydrogen atoms on them will significantly deform the geometry. On the other hand, we found that for the charged models the calculations are increasingly difficult to converge as the size grows. We should take into account that in real working conditions, the charge is counter-balanced by the electrolyte ions and solvent molecules, which are not explicitly included in our calculations. In some specific cases, we have made an estimation of solvation effects through a polarization continuum model (PCM). All the structures were fully optimized prior to calculating the electronic absorption spectra.

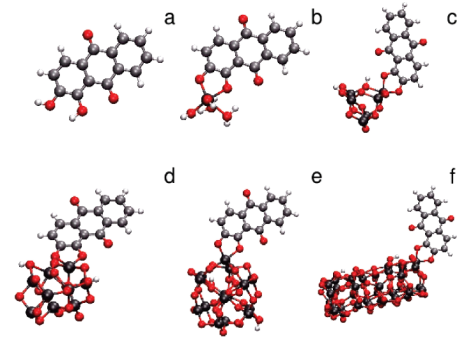

Figure 1. Optimized geometries for free alizarin (a) and adsorbed alizarin on several models (b−f): minimal model U_1, U_6, U_9, U_{15}, and U_{38}, respectively.

2.2. Electronic Absorption Spectra: TD-DFT in Real Time. The electronic absorption spectra were simulated from TD-DFT calculations through two sets of complementary calculations. Although it is known that TD-DFT can significantly underestimate the energies of long-range charge transfer states, that is not the case with the present calculation, in which the photoexcited state shows a moderate and relatively short-ranged charge transfer.[2] The Gaussian 03 code[21] was used to perform conventional LR-TD-DFT calculations[11] and the SIESTA[22,23] code to perform real time TD-DFT calculations.[15,16] Since the latter method has been less used, we include a detailed description in this subsection.

In the simplest case, the lowest band observed in an experimental electronic absorption spectrum comes from a HOMO to LUMO excitation. In the traditional LR-TD-DFT method, a key input parameter is the number of excitations to be included in the calculation. When the excitation that is responsible for the main band in the spectrum is the HOMO−LUMO or mixed with excitations from an occupied orbital close to the HOMO to a virtual orbital close to the LUMO (i.e: HOMO−1 to LUMO, HOMO to LUMO+1,

etc.), then only a small number of excitations have to be included in the calculation. However, when there are molecular orbitals between the initial and the final state of the electronic excitation (i.e: HOMO to LUMO+15), then a large number of excitations will be energetically possible at a lower energy than responsible for the main band. These transitions have usually negligible intensities but have to be explicitly included in the calculations (by allowing a larger number of excitations). As a rule of thumb, if the excitation is from the HOMO orbital to the LUMO+N, the number of excitations to be included is N^2. In the free alizarin molecule, the transition is basically HOMO to LUMO; however, when the molecule is adsorbed, there are many states in between the origin and the destiny of the excitation because of the presence of the cluster. As a consequence, performing a conventional (frequency domain) LR-TD-DFT for large systems becomes prohibitive at a certain size (see the Results section for a case with definite numbers).[24,25] In contrast, the "real time" TD-DFT method generates all the possible excitations at the same time (by applying an electric field to the molecule). The spectrum is calculated from a molecular dynamic simulation and extends to very high excitations (although the spectrum has no real meaning above the ionization energy). The method is not computationally cheap for small systems, as it requires relatively long simulation times, but becomes competitive against the traditional one as the size of the system grows. One disadvantage of this approach is that we cannot fully characterize the nature of the different transitions because the implementation of the method is based on electron density, and there is no information about the excited states wave functions.

The method we have employed[16] involves the description of the electronic states using a linear combination of atomic orbitals (LCAO). Because the size of the LCAO basis is small, the TD-DFT calculations can be done efficiently using the techniques described below. The use of the LCAO basis leads to matrices with a size considerably smaller than when other basis sets are used or when real-space grid methods are employed. The scheme is based on the SIESTA code,[22] which is used to compute the initial wave functions and the Hamiltonian matrix for each time step. Core electrons are replaced by norm-conserving pseudopotentials[26] in the fully nonlocal Kleinman−Bylander[27] form, and the basis set is a general and flexible linear combination of numerical atomic orbitals (NAOs), constructed from the eigenstates of the atomic pseudopotentials.[28−30] The NAOs are confined, being strictly zero beyond certain radii. In addition, the electron wave functions and density are projected onto a real-space grid in order to calculate a certain contribution to the Hamiltonian matrix, such as the Hartree and exchange-correlation terms (details are given in ref 22).

We carry out the calculations in the time domain, explicitly evolving the wave functions, following the approach of ref 16. We consider as an initial state a bound system in a finite electric field; i.e., the Hamiltonian includes a perturbation $\Delta H = -E \cdot x$. For the linear response calculations in the present work, we have set the value of this field to 0.1 V/Å. The system is solved for the ground state using standard time independent DFT. Then, we switch off the electric field at time $t = 0$, and for every subsequent time step we propagate the occupied Kohn−Sham eigenstates by solving the time-dependent Kohn−Sham equation

$$i\hbar\frac{\partial\psi}{\partial t} = H\psi \tag{1}$$

where H is the time-dependent Hamiltonian given by

$$H = -\frac{\hbar^2}{2m}\nabla^2 + V_{\text{ext}}(r,t) + e^2\int\frac{\rho(r',t)}{|r-r'|}\mathrm{d}r' + V_{\text{xc}}[\rho](r,t) \tag{2}$$

with $V_{\text{ext}}(r,t)$ being the external (ionic) potential, $\rho(r,t)$ being the electron density, and $V_{\text{xc}}[\rho](r,t)$ being the exchange-correlation potential. The calculation of the exchange-correlation potential is done using the general gradient approximation (GGA). For every time step, we propagate the wave function using a Crank−Nicholson scheme,[16] and from the new wave functions we construct the new density matrix. The electron density is then obtained and used for the calculation of the Hamiltonian in the new cycle and to calculate the dipole moment $D(t)$. After a Fourier transformation, we obtain the elements of the frequency-dependent polarizability tensor $\alpha_{ij}(\omega)$, which defines the first order response of the system: $D(\omega) = \alpha(\omega)\,E(\omega)$. Using a step function external electric field $E(t) = E\,\Theta(-t)$, we have

$$Im[\alpha(\omega)] = \omega\frac{Re[D(\omega)]}{E} \tag{3}$$

The polarizability determines the optical properties and in particular can be used to calculate the dipole strength function: $S(\omega)$

$$S(\omega) = \frac{2m}{\pi e^2\hbar}\omega\, Im[\alpha(\omega)] \tag{4}$$

The dipole strength function, $S(\omega)$, is proportional to the photoabsorption cross-section and allows for a direct comparison with experiments.

2.3. Technical Details. The Gaussian 03 calculations were performed using two different functionals, B3LYP and PBE, and the 6-31G** basis set. To analyze the solvent effect, we have done the calculations both in the gas phase and containing the methanol solvation effect using the polarizable continuum model (PCM). When necessary, up to the 100 lowest singlet transitions were included in the calculations. The SIESTA calculations were performed using the PBE generalized gradient approach functional together with Troullier−Martins pseudopotentials and an auxiliary real-space grid equivalent to a plane-wave cutoff of 130 Ry. A nonstandard DZP basis set of NAOs has been used.[31] A time step of 1.5×10^{-3} fs was used for the time evolution, and the simulation was carried out for a total time of 60 fs, allowing for an appropriate energy conservation.

3. Results

We start this section with the simulated electronic absorption spectrum of neutral free alizarin (model Aliz-2H). The computed spectrum from real-time TD-DFT calculations is reported in Figure 2a. As can be seen, the lowest band

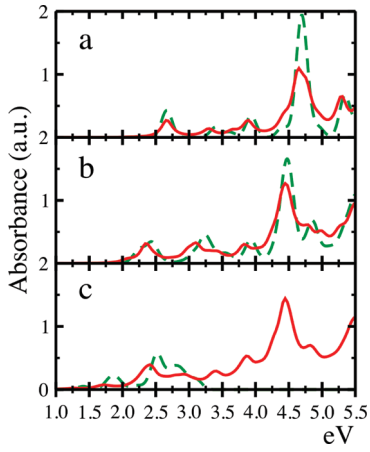

Figure 2. Comparison between conventional (frequency domain) and real-time TD-DFT (red full line) theoretical spectra. From top to bottom: the free alizarin and the adsorbed alizarin on the U_1 and U_6 models.

Table 1. Lowest Band Energies (eV) for Free and Adsorbed Alizarin from Standard (Frequency Domain) TD DFT Calculations Using the PBE and B3LYP Functionals, with and without Including the Solvent Effect through a PCM Model[a]

model	PBE	B3LYP	PBE (PCM)	B3LYP (PCM)
Aliz-2H	2.67 (−0.21)	3.25 (0.37)	2.44 (−0.44)	2.99 (0.11)
Aliz-2H−U_1($2H_2O$)	2.26 (−0.21)	2.96 (0.49)	2.19 (−0.28)	2.63 (0.16)
Aliz-2H−U_6	2.48 (0.01)	2.99 (0.52)		

[a] Experimental bands for free and adsorbed alizarin are at 2.88 eV and ∼2.47 eV, respectively (differences from the experimental data in parentheses).

appears at 2.67 eV, in agreement with the experimental measurement at 2.88 eV. This band is followed by a series of low intensity features and ends with a strong absorption at about 4.65 eV. In order to compare this result with that obtained from LR-TD-DFT calculations, we also report in Figure 2a the spectrum estimated using the same exchange-correlation functional, PBE (see also Table 1). As can be observed, the similarity is remarkable despite the differences in the approaches (basis sets and all-electrons versus pseudopotentials).[32]

Bonding the dye to a titania cluster induces a red-shift of the lowest band, as observed in the two series of spectra reported in Figure 2b and c that correspond to the minimal model Aliz-2H−U_1 (2H2O) and a medium sized cluster, Aliz-2H−U_6, respectively. The estimated red shift is 0.31 and 0.27 eV, in good agreement with the experiment (0.41 eV). With the aim of extending the above comparison to these models, these plots also include the spectra obtained from standard TD-DFT approach. In the case of the minimal model (Figure 2b), the agreement also is notorious, while for model Aliz-2H−U_6 some differences are clearly observed, mainly in the upper energy region of the spectrum (above 3.5 eV). It is worth noting that the conventional spectra extend only to a small energy range because of the limited number of transitions included in the calculation. For instance, the number of excitations to reach the energy of the main band grows from 3 in the smallest model to 56 in the Aliz-2H−U_6 model. From our calculations, we estimate that, to reach the main band energy, more than 300 excitations should be included in the U_{15} model and more than 1000 in the U_{38} case. This is due to the large number of virtual orbitals located on the cluster that produces electronic transitions with negligible intensities (see Table 2 and Figure 5). Since in our calculations we have limited the maximum number of excitations to 100, the upper energy region of the spectrum is inadequately described, and, in fact, that is why the spectrum suddenly fades at 3.35 eV in the case of model Aliz-2H−U_6.

An additional point to bear in mind in the analysis and comparison with the experimental data concerns the solvent effects as well as the choice of the exchange-correlation functional. The functional choice is the key parameter when calculating the electronic spectra (Table 1). The position of the main peak moves to higher energies when passing from the PBE to the B3LYP functional. The energy increments are 0.58, 0.70, and 0.49 eV for the three models here considered. Compared to the experimental spectra, the PBE functional underestimates the transition energy while the values obtained with the hybrid B3LYP functional appear overestimated. The inclusion of solvent effects through a PCM model tends to reduce further the excitation energies (about 0.2−0.3 eV). Therefore, the PBE frequencies are in worse agreement and the B3LYP frequencies in better agreement when including solvent effects.

The overall behavior of the real time TD-DFT spectra for all the models we have considered is summarized in Figures 3 and 4. In general, the simulated spectra look similar, and as can be seen, upon adsorption there is a significant red shift of the main band of alizarin which moves from 2.67 eV for the free molecule to 2.21 eV when adsorbed on the U_{38} cluster (−0.46 eV theoretical shift compared to the −0.41 experimental shift). There is also an increase in the absorbance in the visible region because of the high number of low energy excitations within the cluster. The spectrum of our benchmark model, Aliz−U_{38}-2H, reported in detail in Figure 3, shows broad bands centered at 2.21, 3.27, and 4.2 eV. These bands also appear for other models, although we note that there are small changes in the position and relative intensities. In general, the smaller the model, the more featured the spectra. As the system grows bigger, the bands in the spectra become wider and less resolved because the number of involved excitations increases. This is in agreement with what is found in experiments and also reflects the fact that the model system is switching from having discrete energy levels to energy bands. The main feature of the spectra (the red shift upon adsorption) is already reproduced, albeit qualitatively, by the minimal model. However, to account for the delocalization of the excitations over the titania particle, the detailed analysis of the electronic transitions shows that larger cluster models are needed.

In Figure 5, the computed Kohn−Sham orbital energy levels for several models in the relevant energy window are shown. The HOMO orbital energy has been taken as a reference to allow a better comparison and has been set to zero. In the free alizarin, the most intense contribution to the lowest energy band comes from an excitation from the

Table 2. Assignments of Electronic Excitations for Free Alizarin and Adsorbed on U_1 and U_6 Models[a]

transition energy (eV), excitation number	oscillator strength	wave function
		Free Alizarin
2.67 (3)	0.0856	H−1→L (0.63), H−1→L+3 (−0.13), H−3→L+2 (0.11)
		U_1 Model
2.18 (2)	0.0098	H→L+1 (0.58), H→L (0.31), H−1→L (−0.19)
2.26 (3)	0.0282	H→L+2 (0.46), H→L (−0.32), H−1→L+1 (−0.24), H→L+1 (0.20), H−1→L (0.16), H−1→L+2 (−0.15)
2.29 (4)	0.0105	H−1→L+1 (0.62), H→L+2 (0.19), H→L (−0.17), H−1→L+2 (0.16)
		U_6 Model
2.48 (56)	0.0368	H→L+10 (0.39), H−3→L+6 (−0.30) H→L+11 (0.20), H→L+13 (−0.19), H−2→L+11 (0.18), H−2→L+12 (0.17), H→L+14 (−0.12)
2.53 (58)	0.0147	H−5→L+4 (0.58), H−3→L+6 (−0.27), H−1→L+14 (0.18), H−2→L+10 (0.11), H→L+10 (−0.11)
2.53 (59)	0.0177	H−5→L+5 (0.49), H−5→L+4 (−0.30), H−3→L+6 (−0.30), H−1→L+14 (0.17), H→L+10 (−0.12)
2.53 (60)	0.0213	H−5→L+3 (0.50), H−3→L+6 (0.32), H−5→L+4 (0.24), H−1→L+14 (−0.19), H→L+10 (0.13), H−2→L+12 (−0.11)
2.56 (63)	0.0214	H−1→L+14 (0.60), H−3→L+6 (0.17), H→L+10 (0.16), H→L+14 (0.14), H−2→L+10 (−0.13)

[a] Only selected transitions with enough oscillator strength around the main peak are included (H stands for HOMO and L for LUMO).

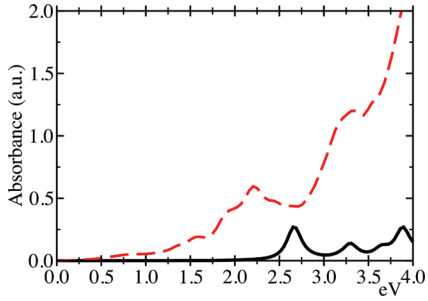

Figure 3. Real-time TD-DFT theoretical spectra for free alizarin (black full line) and adsorbed on U_{38}.

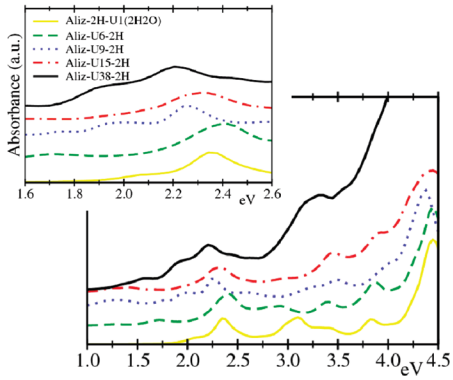

Figure 4. Real-time TD-DFT theoretical spectra for the adsorbed alizarin on several models. Bottom to top: U_1, U_6, U_9, U_{15}, and U_{38}. The spectra have been shifted along the *y* axis to allow for a better comparison. Inset: a zoom in of the main band energy region.

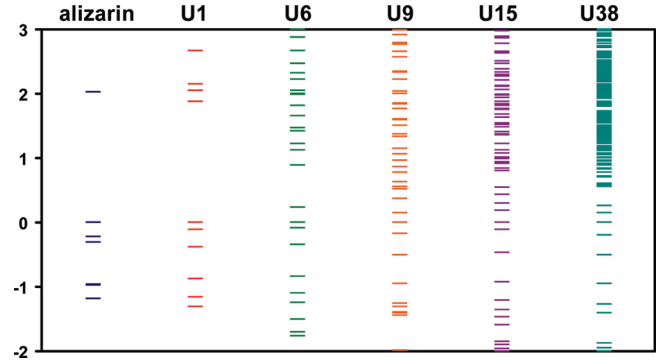

Figure 5. Molecular orbital energies for the ground state. From left to right: the free alizarin and the adsorbed U_1, U_6, U_9, U_{15}, and U_{38} models. For the sake of comparison, the levels have been shifted to set the HOMO energy as the zero energy.

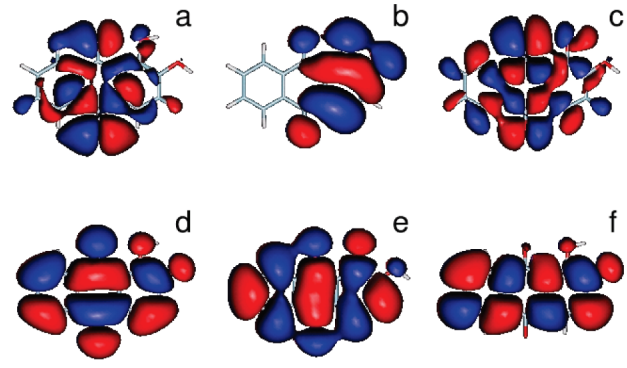

Figure 6. Selected frontier occupied and virtual molecular orbitals of free alizarin. (a) HOMO−2, (b) HOMO−1, (c) HOMO, (d) LUMO, (e) LUMO+1, (f) LUMO+2.

HOMO−1 to the LUMO (Table 2). This is in agreement with previous theoretical calculations making use of the PW91 functional.[4] The HOMO−1 orbital is a π orbital localized over the hydroxyl part of the molecule (Figure 6). The lone electron pairs of the hydroxyl and quinone oxygens contribute to this orbital. The LUMO is distributed over the whole molecule ring. The difference in the dipole moments between the ground and excited states was experimentally quantified as 4.4 D, which reflects the significant intramolecular transfer of electronic charge in the electronic transition.[3]

After binding to titanium, there is a redistribution of electron density. In the minimal model, the relevant excitations that form the main band start from the HOMO or

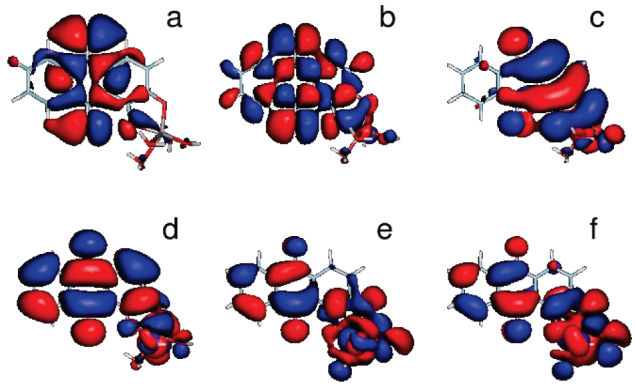

Figure 7. Selected frontier occupied and virtual molecular orbitals of the minimal model. (a) HOMO−2, (b) HOMO−1, (c) HOMO, (d) LUMO, (e) LUMO+1, (f) LUMO+2.

HOMO−1 to the LUMO, LUMO+1, and LUMO+2 since the orbital energies of these occupied and virtual states respectively are close in energy (Table 2 and Figure 5). Since the electronic states shown in Figure 7 extend over both the molecule and the Ti, there are more excitations producing a nonzero contribution to the main band. The HOMO and LUMO resemble those of the free molecule (HOMO−1 and HOMO switch positions when passing to the minimal model). However, in every case, there is a noticeable contribution from the Ti atom. This is especially true in the LUMO+1 and LUMO+2 where the d orbitals of Ti play a significant role. The occupied electronic states are mainly localized on the alizarin molecule whereas the virtual electronic states show a larger contribution from the Ti 3d orbitals; that is, the molecular orbitals extend over the whole system. It has been suggested from Stark effect measurements that the excited state of alizarin would be essentially localized on the dye molecule, and the nanoparticle electric field would cause the absorption band shift.[3] This does not seem to agree with our calculations, since we conclude that the shift in the spectrum of the minimal model seems to be related to a stabilization of the acceptor states relative to the donor states because of the hybridation.

When the cluster contains several titanium atoms, the electronic wave function may spread over the whole system so becoming more stable than the orbital localized on the alizarin. In Figure 8, some relevant molecular orbitals for the Aliz-2H−U_6 model are shown. These orbitals have been chosen because they are the most important in contributing to the lowest energy band. In this case (Table 2), the band is made of several optical transitions, and each of them corresponds to several pairs of donor and acceptor orbitals. The occupied orbitals that contribute most are HOMO−5, HOMO−3, HOMO−1, and HOMO. They all are mainly localized on the alizarin, although there is some minor contribution from the Ti atoms close to the molecule (i.e., in the HOMO). On the other hand, LUMO+10 and LUMO+11 are the main contributors to the most intense transition and are localized on the alizarin. They resemble the LUMO in the free molecule. LUMO+6, which shows an important contribution from the alizarin, is responsible for a small band at about 1.9 eV (Figure 2). From Table 2 it is clear that LUMO, LUMO+1, LUMO+2, LUMO+7,

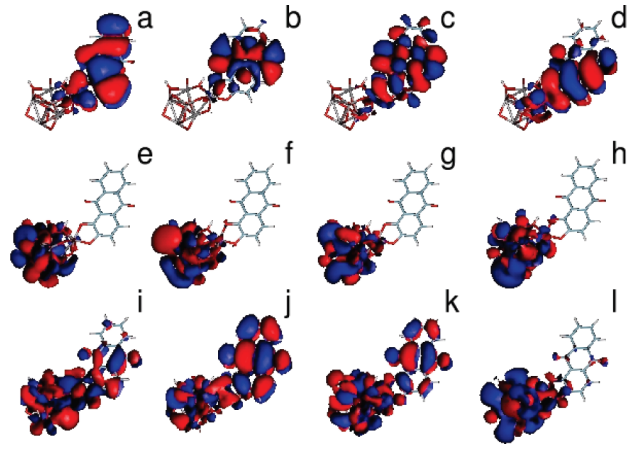

Figure 8. Selected frontier occupied and virtual molecular orbitals of the U_6 model. (a) HOMO−3, (b) HOMO−2, (c) HOMO−1, (d) HOMO, (e) LUMO, (f) LUMO+1, (g) LUMO+2, (h) LUMO+3, (i) LUMO+6, (j) LUMO+10, (k) LUMO+11, and (l) LUMO+12.

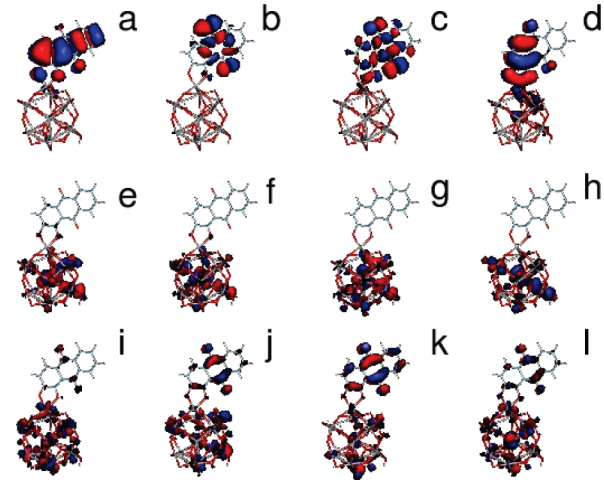

Figure 9. Selected frontier occupied and virtual molecular orbitals of the U_{15} model. (a) HOMO−3, (b) HOMO−2, (c) HOMO−1, (d) HOMO, (e) LUMO, (f) LUMO+1, (g) LUMO+2, (h) LUMO+3, (i) LUMO+30, (j) LUMO+32, (k) LUMO+33, and (l) LUMO+35.

LUMO+8, and LUMO+9 do not participate in the transitions that make up the main band because they are totally localized on the cluster, so their overlap with the occupied orbitals is negligible.

On the other hand, when the cluster size becomes larger, the virtual orbitals close to the HOMO are well localized at the center of the cluster (see LUMO and LUMO+1 in Figure 9). The energies of these orbitals show some "molecular" character since they are discrete. Above these states, there are manifold states delocalized on the whole cluster that become closer to a band (a continuum of states) for the U_{38} model (Figure 5). It is worth notice that there is an increasing number of virtual orbitals between the HOMO and LUMO of the free alizarin as the system grows bigger. The former LUMO transforms into LUMO+10 for the U_6, LUMO+17 for the U_9, LUMO+33 for the U_{15}, and about LUMO+90 for the U_{38}. In every case, the energy difference remains about 2 eV, which makes the main band in the spectrum

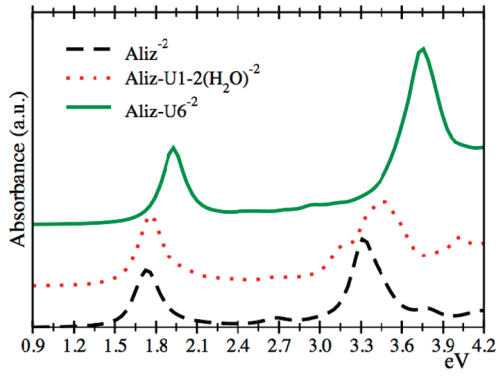

Figure 10. Real-time TD-DFT theoretical spectra for isolated dianion alizarin (black dashed line) and adsorbed on U_1 (red dot line) and U_6 (green full line).

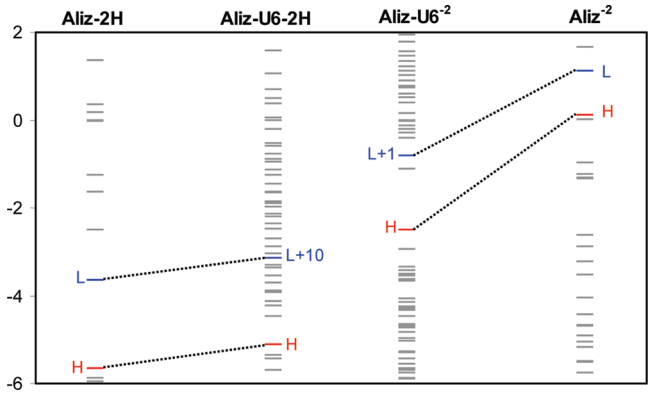

Figure 11. Molecular orbital energies of neutral and dianion alizarin forms isolated and adsorbed on the U_6 model.

almost unaltered in position (Figure 4). The number of excitations below the main transition grows substantially, although the intensities are usually close to zero.

An additional point we have considered concerns the fact that the lowest absorption in the alizarin electronic spectrum moves when the pH of the solution changes. Thus, in an ethylene glycol/water solution the position of this peak is 2.85, 2.34, and 2.17 eV at pH of 3, 10, and 14 respectively.[3] This shift is interpreted in terms of the actual form of alizarin that can be neutral, monoanionic and dianionic depending on the pH. To analyze this point additional calculations for negatively charged models were performed for both isolated and supported alizarin species. For isolated alizarin, the lowest peak for the dianion form is computed at 1.75 eV and moves to 1.87 eV for the monoanion species (0.8 eV below the neutral), in agreement with the experimental trend. When the dianion species is supported on a titania cluster, a blue shift of this band is observed as shown in Figure 10, where the spectra of the dianion form isolated and bound to U1 and U6 models are depicted. This behavior agrees with the experimental shift observed in the spectra of the TiO_2−alizarin complex at pH = 11.[3] The electronic changes involved in these shifts might be understood taking into account the redistribution of the energy levels that happens upon dissociation and adsorption. As shown in Figure 11, double proton dissociation leads to a relative destabilization of HOMO with respect to LUMO (both strongly destabilized). As a consequence, the first band that, as already commented upon, is mainly contributed by this excitation is red-shifted. Upon adsorption, both HOMOs and LUMOs are stabilized, although the lowering of the former is larger. Consequently, the band is blue-shifted. Notice that the stabilization of the alizarin molecular orbitals that occurs upon adsorption is consistent with a larger redistribution of the negative charge over the titania cluster. Such redistribution is more efficient when the size of the cluster increases, and therefore the blue shift for U6 is larger than for U1. Although larger clusters should lead to larger shifts, we could not go further due to convergence problems. Finally, to end this discussion, it is worth noting that although the results are in qualitative agreement with experiments (in the sense that there is a blue shift of the main peak upon adsorption),[3] we should stress again that the system does not include solvent or cationic entities that could counterbalance the net charge on the system.

A final point worth highlighting is that recent experimental work on the electron injection process revealed multiexponential dynamics with different time constants, characteristic of a nonadiabatic process.[7] There were electron transfer events in about 0.1 ps and back electron transfer in 0.2 ps. In addition, a second injection time in about 17 ps and a slow back electron transfer in 1 ns were reported. This observation was explained on the basis of a finite size effect, which could lead to discreteness in the conduction band levels leading to different injection times to different levels within the conduction band.[7] From Figure 5, it is clear how the energy level bands are formed as the system grows while maintaining some discrete levels above the HOMO localized on the cluster.

We speculate that there are electron injections to discrete levels localized on the cluster and to levels corresponding to LUMO in the free molecule. The direct and back electron transfer are fast for the former case, since the levels are localized and the energy difference between donor and acceptor levels is small. On the other hand, in the latter case, the direct electron transfer is slightly slower (the energy difference is larger), whereas the back electron transfer is very slow since the electron wave function is spread over the whole cluster, which favors the transfer of the electron to TiO_2. This second electron transfer is responsible for the solar cell response. The possibility of changing the energy levels by using certain cluster sizes could have a potential use in the design of more efficient organic solar cells.

Conclusions

In this study, we have analyzed the electronic structure and the electronic absorption spectra of neutral alizarin both free and bound to TiO_2 nanoclusters of different sizes. To this aim, we have employed two different implementations of the TD-DFT to simulate the electronic spectra: the time domain and the frequency domain approaches. A first conclusion that can be reached is that, within the range of models we have examined, both methods provide comparable results as far as the basis set and the exchange-correlation functional are similar. This proves that the real-time TD-DFT scheme implemented within the SIESTA code is accurate for this type of system.

For free alizarin, our simulated spectra show a low energy band at 2.67 eV, in agreement with the experimental value (2.88 eV) and previous theoretical work. Upon adsorption, and also in agreement with the experiment, this band features a shift toward lower energies of 0.27−0.46 eV (PBE) depending on the model size. The effect of the size of the TiO_2 nanoparticle has been modeled by using differently sized nanoclusters going from the minimal TiO_4H_4 unit to a $(TiO_2)_{38}$ cluster, for which the estimated red shift is found to be 0.46 eV, in excellent agreement with the experiment (0.41 eV). From the analysis, we conclude that the minimal model is enough to reproduce the main feature in the spectra (a red-shift upon binding). Larger clusters do not much modify this picture since the energy difference between the HOMO and the orbital corresponding to the free molecule LUMO remains almost the same (i.e., the main excitation stays almost unchanged). However, the electronic structure of the system does change for larger systems. The virtual orbital on the alizarin responsible for the excitation moves from being below the "conduction band" for the minimal model to being well into the conduction band for larger clusters. In addition, we note that there are finite size effects that create discrete levels localized on the clusters. This may have important consequences for the dynamics of electron transfer. From our study, we regard the a unit of $(TiO_2)_6$ as the smallest nanocluster model able to simulate semiquantitatively all the features in the electronic structure of the system.

Acknowledgment. This work was funded by the Spanish Ministerio de Ciencia e Innovación, MICINN, projects MAT2008-4918, CSD2008-0023, FIS2009-12721-C04-01, and CSD2007-00050. R.S.A. thanks the Junta de Andalucía for a predoctoral grant (P08-FQM-3661 and EXC/2005/FQM-1126). Part of the calculations have been carried out at the Barcelona Supercomputing Center—Centro Nacional de Supercomputación (Spain).

References

(1) Duncan, W. R.; Prezhdo, O. V. *Annu. Rev. Phys. Chem.* **2007**, *58*, 143.

(2) Duncan, W. R.; Stier, W. M.; Prezhdo, O. V. *J. Am. Chem. Soc.* **2005**, *127*, 7941.

(3) Nawrocka, A.; Krawczyk, S. *J. Phys. Chem. C* **2008**, *112*, 10233.

(4) Duncan, W. R.; Prezhdo, O. V. *J. Phys. Chem. B* **2005**, *109*, 365.

(5) Duncan, W. R.; Craig, C. F.; Prezhdo, O. V. *J. Am. Chem. Soc.* **2007**, *12*, 9–8528.

(6) Duncan, W. R.; Prezhdo, O. V. *J. Am. Chem. Soc.* **2008**, *130*, 9756.

(7) Kaniyankandy, S.; Verma, S.; Mondal, J. A.; Palit, D. K.; Ghosh, H. N. *J. Phys. Chem. C* **2009**, *113*, 3593.

(8) Huber, R.; Moser, J. E.; Grätzel, M.; Wachtveitl, J. *J. Phys. Chem. B* **2002**, *106*, 6494.

(9) Huber, R.; Spörlein, S.; Moser, J. E.; Grätzel, M.; Wachtveitl, J. *J. Phys. Chem. B* **2000**, *104*, 8995.

(10) Duncan, W. R.; Prezhdo, O. V. *J. Phys. Chem. B* **2005**, *109*, 17988.

(11) Casida, M. E. Recent Developments and Applications of Modern Density Functional Theory. In *Theoretical and Computational Chemistry*; Seminario, M., Ed.; Elsevier: Amsterdam, 1996; Vol *4*, p 391.

(12) Kondov, I.; Wang, H.; Thoss, M. *Int. J. Quantum Chem.* **2006**, *106*, 1291.

(13) Guo, Z.; Liang, W. Z.; Zhao, Y.; Chen, G. H. *J. Phys. Chem. C* **2008**, *112*, 16655.

(14) Stratmann, R. E.; Scuseria, G. E.; Frisch, M. J. *J. Chem. Phys.* **1998**, *109*, 8218.

(15) Yabana, K.; Bertsch, G. F. *Phys. Rev. B* **1996**, *54*, 4484.

(16) Tsolakidis, A.; Sánchez-Portal, D.; Martin, R. M. *Phys. Rev. B* **2002**, *66*, 235416.

(17) Zhang, H.; Banfield, J. F. *J. Mater. Chem.* **1998**, *8*, 2073.

(18) Qu, Z.; Kroes, G. *J. Phys. Chem. B* **2006**, *110*, 8998.

(19) Hamad, S.; Catlow, C. R. A.; Woodley, S. M.; Lago, S.; Mejías, J. A. *J. Phys. Chem. B* **2005**, *109*, 15741.

(20) Lundquist, M. J.; Nilsing, M.; Persson, P.; Lunell, S. *Int. J. Quantum Chem.* **2006**, *106*, 3214.

(21) Frisch, M. J.; Trucks, G. W.; Schlegel, H. B.; Scuseria, G. E.; Rob, M. A.; Cheeseman, J. R.; Montgomery, J. A., Jr.; Vreven, T.; Kudin, K. N.; Burant, J. C.; Millam, J. M.; Iyengar, S. S.; Tomasi, J.; Barone, V.; Mennucci, B.; Cossi, M.; Scalmani, G.; Rega, N.; Petersson, G. A.; Nakatsuji, H.; Hada, M.; Ehara, M.; Toyota, K.; Fukuda, R.; Hasegawa, J.; Ishida, M.; Nakajima, T.; Honda, Y.; Kitao, O.; Nakai, H.; Klene, M.; Li, X.; Knox, J. E.; Hratchian, H. P.; Cross, J. B.; Bakken, V.; Adamo, C.; Jaramillo, J.; Gomperts, R.; Stratmann, R. E.; Yazyev, O.; Austin, A. J.; Cammi, R.; Pomelli, C.; Ochterski, J. W.; Ayala, P. Y.; Morokuma, K.; Voth, G. A.; Salvador, P.; Dannenberg, J. J.; Zakrzewski, V. G.; Dapprich, S.; Daniels, A. D.; Strain, M. C.; Farkas, O.; Malick, D. K.; Rabuck, A. D.; Raghavachari, K.; Foresman, J. B.; Ortiz, J. V.; Cui, Q.; Baboul, A. G.; Clifford, S.; Cioslowski, J.; Stefanov, B. B.; Liu, G.; Liashenko, A.; Piskorz, P.; Komaromi, I.; Martin, R. L.; Fox, D. J.; Keith, T.; Al-Laham, M. A.; Peng, C. Y.; Nanayakkara, A.; Challacombe, M.; Gill, P. M. W.; Johnson, B.; Chen, W.; Wong, M. W.; Gonzalez, C.; Pople, J. A. *Gaussian 03*; Gaussian, Inc.: Wallingford, CT, 2003.

(22) Soler, J. M.; Artacho, E.; Gale, J. D.; García, A.; Junquera, J.; Ordejón, P.; Sánchez-Portal, D. J. *Phys. Condens. Matter.* **2002**, *14*, 2745.

(23) Sánchez-Portal, D.; Ordejón, P.; Artacho, E.; Soler, J. M. *Int. J. Quantum Chem.* **1997**, *67*, 453.

(24) Different schemes have been proposed, however, to calculate optical spectra in the frequency domain, that rely on iterative methods to estimate the full spectrum of large systems with moderate computational workload (see ref 25). These are still not broadly used and have not been considered in our study.

(25) Walker, B. A. M.; Saitta, A. M.; Gebauer, R.; Baroni, S. *Phys. Rev. Lett.* **2006**, *96*, 113001.

(26) Troullier, N.; Martins, J. L. *Phys. Rev. B* **1991**, *43*, 1993.

(27) Kleinman, L.; Bylander, D. M. *Phys. Rev. Lett.* **1982**, *48*, 1425.

(28) Artacho, E.; Sánchez-Portal, D.; Ordejón, P.; García, A.; Soler, J. M. *Int. J. Quantum Chem. Status Solidi B* **1999**, *215*, 809.

(29) Junquera, J.; Paz, O.; Sanchez-Portal, D.; Artacho, E. *Phys. Rev. B* **2001**, *64*, 235111.

(30) Anglada, E.; Soler, J. M.; Junquera, J.; Artacho, E. *Phys. Rev. B* **2002**, *66*, 205101.

(31) The Ti atom basis set consists of 15 basis functions: two radial functions to represent the 4s electrons with cutoff radii 6.10 and 5.12 au, one radial function for the 4p orbitals with radius 3.11 au, and two functions for the 3d shell with radii 5.95 and 4.75 au. Oxygen electrons were described with 13 functions: two for the 2s shell with confinement radii 4.46 and 2.51 au, two functions for the 2p orbital with radii 6.17 and 2.33 au, and one function for 3d polarization shell with radius 5.06 au. The C atom basis set consists of 13 basis functions: two for the 2s states with radii 5.52 and 3.10 au, two for the 2p orbital with radii 6.91 and 3.03 au, and one function for the 3d polarization shell with radius 5.12 au. Finally, for the H atom, five functions were used: two radial functions for the 1s shell with radii 4.95 and 1.77 au and one function for the 2p polarization shell with a 5.07 au radius.

(32) The standard TD-DFT (Gaussian 03 code) spectrum was fitted by assigning a Gaussian function to each electronic excitation frequency with an area proportional to the oscillator strength of that excitation. A single width parameter was chosen so the band broadening was similar to that in real time TD-DFT spectra.

CT100289T